Journal of Power Sources 222 (2013) 10–14

Contents lists available at SciVerse ScienceDirect

Journal of Power Sources

journal homepage: www.elsevier.com/locate/jpowsour

Short communication

$La_{0.8}Sr_{0.2}Ga_{0.8}Mg_{0.2}O_{3-\delta}$ thin films for IT-SOFCs: Microstructure and transport properties correlation

Nan Yang [a,b], Alessandra D'Epifanio [a,*], Elisabetta Di Bartolomeo [a], Chiara Pugnalini [a], Antonello Tebano [b], Giuseppe Balestrino [b], Silvia Licoccia [a]

[a] Department of Chemical Science and Technologies & NAST Center, University of Rome, Tor Vergata, Via della Ricerca Scientifica 1, 00133 Rome, Italy
[b] CNR-SPIN & Dipartimento di Informatica, Sistemi e Produzione, University of Rome Tor Vergata, Via del Politecnico 1, 00133 Rome, Italy

HIGHLIGHTS

- Deposition of $La_{0.8}Sr_{0.2}Ga_{0.8}Mg_{0.2}O_3$ on (001) $NdGaO_3$ and $SrTiO_3$ buffered (001) MgO substrates.
- Structural and microstructural analysis of the films.
- Transport properties analysis.
- Correlation between the film thickness, the grain boundary concentration, and the conductivity.

ARTICLE INFO

Article history:
Received 18 May 2012
Received in revised form
18 August 2012
Accepted 22 August 2012
Available online 1 September 2012

Keywords:
LSGM films
PLD
Microstructure
Electrochemical characterization

ABSTRACT

Highly textured $La_{0.8}Sr_{0.2}Ga_{0.8}Mg_{0.2}O_3$ (LSGM) films with columnar structure were grown by pulsed laser deposition on (001) $NdGaO_3$ and $SrTiO_3$ buffered (001) MgO substrates. Combined analysis of the films structure and morphology and EIS measurements showed that the transport properties are mainly limited by perpendicular grain boundaries effects. Increasing the film thickness, columnar nanosized grains tend to coalesce leading to a decrease of grain boundary concentration, hence to enhanced conductivity.

1. Introduction

Solid oxide fuel cells (SOFCs) operating at low temperatures are very promising devices for sustainable energy production both for stationary and mobile applications [1]. A viable means to reduce SOFCs operating temperature is to produce electrolytes in the form of thin films [2–4]. Pulsed laser deposition (PLD) is particularly promising amongst the different film deposition techniques because of its ability in reproducing complex target compositions onto the film [5]. Moreover, the deposition can be carried out at relatively low temperature values (≈700 °C) avoiding elemental interdiffusion at the substrate/film interface and preventing the detrimental formation of extra-phases at the electrolyte/electrode interfaces. Strontium and magnesium doped lanthanum gallate ($La_{1-x}Sr_xGa_{1-x}Mg_xO_{3-\delta}$, LSGM) perovskites have very large ionic conductivity (~0.02 Scm^{-1} at 600 °C, almost one order of magnitude larger than that of YSZ), oxygen transport number close to unity, good chemical stability over a wide oxygen partial pressure range, good mechanical strength and thus are widely considered excellent candidates as electrolytes operating at intermediate temperatures (IT) (400–600 °C) [6–8]. In comparison to doped-ceria, which is another promising electrolyte for IT applications, LSGM shows a negligible electronic conduction (at $T < 1000$ °C). The main drawback of LSGM perovskite is the cation interdiffusion occurring during the sintering process across the interface between electrolyte and anodic or cathodic substrates, such as the commonly used GDC/NiO or strontium-doped rare earth cobaltites, with the consequent formation of insulating phases. LSGM has been fabricated in the form of thin films by PLD both on anode materials and on Al_2O_3 and $SrTiO_3$ substrates [9,10]. However, in neither case the correlation between microstructure and transport properties was deeply investigated.

* Corresponding author. Tel.: +39 06 7259 4737; fax: +39 06 7259 4328.
E-mail address: alessandra.d.epifanio@uniroma2.it (A. D'Epifanio).

0378-7753/$ – see front matter © 2012 Elsevier B.V. All rights reserved.
http://dx.doi.org/10.1016/j.jpowsour.2012.08.072

Thin films and heterostructures offer the possibility of investigating interface and grain boundary effects due to space charge layers (SCL) or mechanical strain [11]. With the aim of gaining a deeper understanding of the microstructure/transport properties correlation in LSGM thin films, we deposited by PLD films of different thickness on two different substrates.

Among the commonly used substrates, (110)-oriented $NdGaO_3$ (orthorhombic perovskite structure, $a = b = 3.863$ Å, $c = 3.854$ Å in the pseudocubic cell) and (001)-oriented MgO (cubic rock-salt structure, $a = 4.21$ Å) were chosen because of their low residual mixed electronic/ionic conductivity in the intermediate temperatures range, thus allowing reliable transport measurements. The poor lattice match between MgO and LSGM, however, prevents the epitaxial growth: thus LSGM films were deposited on (001) MgO substrates buffered by a thin $SrTiO_3$ (STO) layer about 30 nm thick. Fig. 1 shows a sketch of the epitaxial relationship between the LSGM cubic perovskite, STO cubic perovskite and MgO cubic cell. LSGM and STO have cubic lattice parameters of about $a = 3.93$ Å and 3.91 Å, respectively. Therefore, STO matches quite well the lattice parameter of LSGM. A similar approach has been previously reported for the deposition of epitaxial Sm doped ceria films on MgO substrates [12].

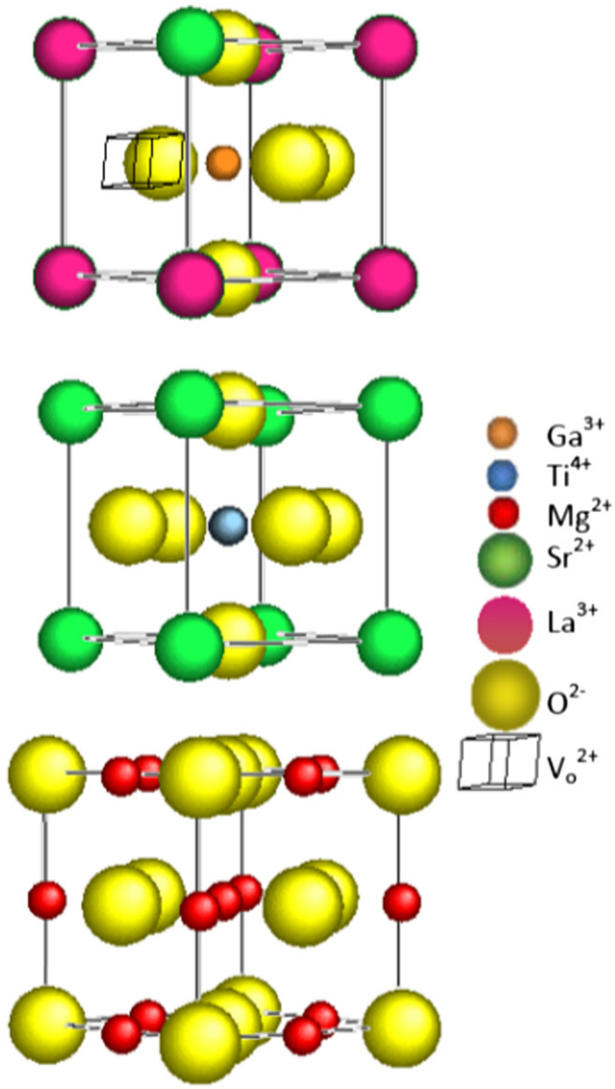

Fig. 1. Schematic sketch of the correlation between the cells of LSGM, STO, and MgO.

2. Experimental

LSGM films having three different thicknesses (100, 500, and 1000 nm) were deposited by PLD on insulating, STO buffered, (001) MgO substrates and 500 and 1000 nm films were grown on $NdGaO_3$ substrates. Targets were prepared from commercial LSGM powders from Praxair, by uniaxially pressing at 250 MPa and sintering at 1500 °C for 10 h. The KrF excimer pulsed laser source ($\lambda = 248$ nm) was operated at 10 Hz, with an energy density of 5 Jcm^{-2}, the substrate temperature was about 600 °C and O_2 pressure was 1 Pa, target–substrate distance was 3 cm. With this set of parameters a deposition rate of about 0.22 Å per laser shot was obtained.

XRD analyses were performed on targets and as-grown films to determine the lattice parameters and to rule out the presence of impurity phases. Scans in the θ–2θ mode and rocking curves were carried out on LSGM/STO/MgO heterostructures and LSGM/$NdGaO_3$ films using: Cu Kα radiation, accelerating voltage: 30 kV, filament current: 30 mA, 10°/minute (scan rate for the theta–2theta scan), 0.5°/minute (scan rate for the theta scan).

Morphological characterization was carried out by field emission scanning electron microscopy (FE-SEM, Leo Supra 35).

The electrochemical characterization of LSGM thin layer was carried out by electrochemical impedance spectroscopy (EIS) using a frequency response analyzer (FRA Solartron 1260), coupled with a dielectric interface (Solartron 1296). Gold electrodes were applied in a two-electrode configuration geometry using a commercial gold paste painted onto the film surface. EIS measurements were recorded in air atmosphere in the temperature range between 700 and 300 °C in the frequency range 1 MHz–0.01 Hz using voltage amplitude of 100–500 mV. The first run of measurements was performed starting from 700 °C, after a long thermal stabilization, and then cooling down to 400 °C. A post deposition annealing was thus performed in the test cell. All EIS measurements were repeated both in cooling and heating runs.

3. Result and discussion

Typical X-ray scans of an LSGM/STO/MgO and LSGM/$NdGaO_3$ films are shown in Fig. 2(a) and (b), respectively. Only the (00*l*) reflections from LSGM are visible in both diffraction patterns,

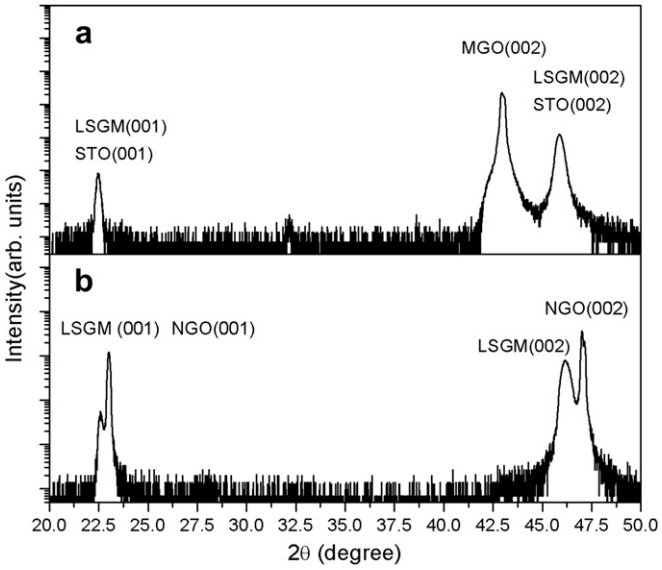

Fig. 2. XRD pattern of as-grown (a) LSGM/STO/MgO and (b) LSGM/$NdGaO_3$ 1000 nm thick.

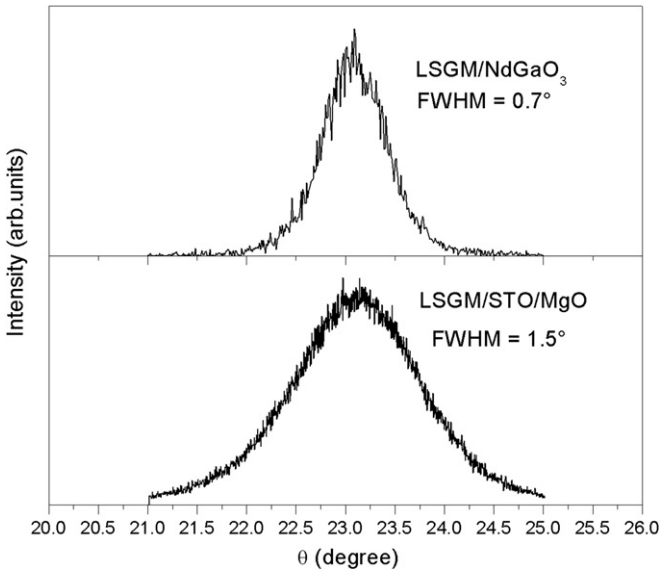

Fig. 3. Rocking-curve scans for as-grown LSGM/$NdGaO_3$ and LSGM/STO/MgO films (1000 nm).

indicating that the film is highly textured along the *c*-axis. In the case of the LSGM/STO/MGO heterostructures (Fig. 2(a)), because of the close values of lattice parameters, the reflection peaks of LSGM films overlap those from the STO buffer. However, the STO buffer layer is too thin to provide a sizeable contribution to the diffracted intensity.

Fig. 3 shows the rocking-curve scans for as-grown LSGM/STO/MgO and LSGM/$NdGaO_3$ films having the same 1 μm thickness. The full width at half-maximum (FWHM) are 1.5° and 0.7°, respectively, hence much larger than both $NdGaO_3$ and MgO substrates (≤0.1°). A better crystallographic quality is obtained for LSGM films deposited on $NdGaO_3$ substrates while LSGM/STO/MgO films show a larger FWHM due to the large lattice misfit, 6.9%, between LSGM and MgO which is only partially compensated by the STO buffer layer.

Fig. 4 shows the FE-SEM surface micrographs of 1000 nm LSGM films on (a) STO/MgO and (b) $NdGaO_3$ substrates. In both cases the film surface appears as fully dense. For LSGM/STO/MgO films the grain size is around 100 nm while for LSGM/$NdGaO_3$ films it is even difficult to detect the grain size because of the very smooth surface, confirming XRD analysis and indicating a better grain boundary match.

Conductivity measurements were carried out in air by EIS (10 MHz–0.01 Hz) in the 400–700 °C temperature range. Gold electrodes were used in planar configuration onto the LSGM film surface. Fig. 5 shows the Arrhenius plots of LSGM/$NdGaO_3$ and LSGM/STO/MgO 1000 nm thick films.

The activation energy (E_a) is the same for both samples and is about 1 eV, typical of oxygen ion conductors, but the film with higher crystallographic quality, LSGM deposited on $NdGaO_3$, shows higher conductivity than the one deposited on STO/MgO. The inset in Fig. 5, shows the impedance spectrum measured at 650 °C for the film on STO/MgO substrate. The spectrum shows a single semicircle, fitted by an RC equivalent circuit, where the resistance *R* is the sum of the bulk and grain boundary contributions. The capacitance *C* is of the order of 10^{-11} F, typical of the insulating substrate and measuring cell (stray capacitance) [11,14]. All investigated films always showed a single semicircle in the Nyquist plot at all temperatures in agreement with relevant literature on epitaxial thin films [10–12].

Fig. 6 shows the rocking curves of LSGM/STO/MgO films having different thickness. The increase of the FWHM value, from 1.5° to 2.1°, with decreasing film thickness, from 1 μm to 100 nm, indicates that the crystallographic disorder increases for thinner films. In the case of LSGM/$NdGaO_3$ films, the rocking curve FWHMs were 0.7° (Fig. 3 for a 1000 nm thick film) and did not show any appreciable change with film thickness.

Fig. 7 shows the FE-SEM micrograph of the surface fracture of the 1 μm thick LSGM/STO/MgO heterostructure where a highly

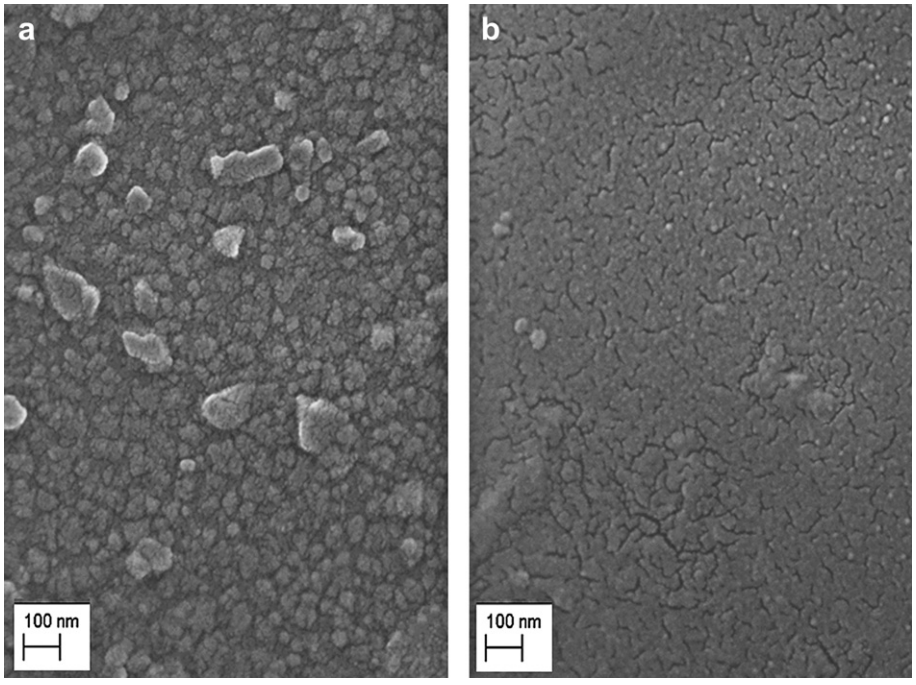

Fig. 4. SEM micrographs (top-view) of 1 μm thick (a) LSGM/STO/MgO and (b) LSGM/$NdGaO_3$ films.

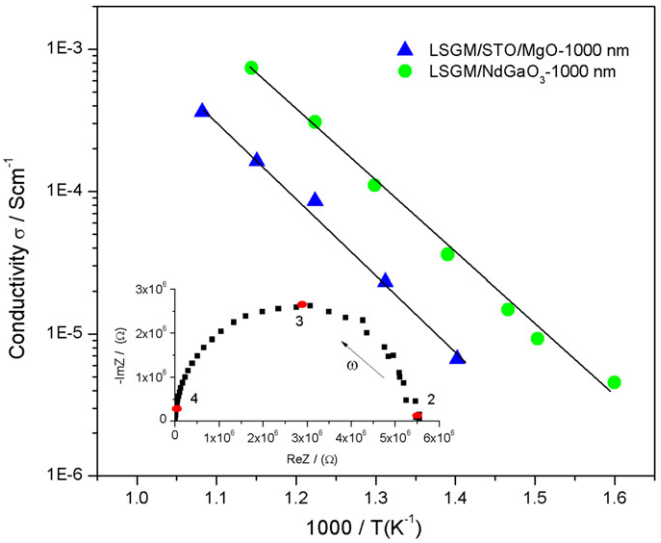

Fig. 5. Arrhenius plots of LSGM/$NdGaO_3$ and LSGM20/STO/MgO 1000 nm thick films. The inset shows the Nyquist plot measured in air at 650 °C for LSGM/STO/MgO.

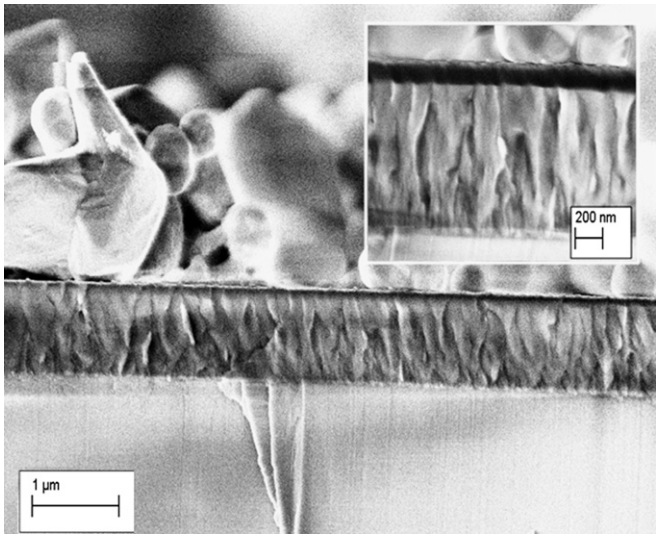

Fig. 7. FE-SEM micrograph (cross-section) of 1 μm thick LSGM/STO/MgO film.

textured columnar structure at the nanometer scale can be clearly identified. Columnar grains tend to coalesce as the growth proceeds resulting in a surface region less defective relative to the interface region. Because of the large misfit between STO and MgO, the STO buffer layer relaxes rapidly becoming very defective: defects propagate through the STO/LSGM interface originating a columnar structure in the LSGM film. This result is in agreement with XRD characterization and shows that thicker films have, on the average, a higher crystallographic order.

The temperature dependent total conductivity is shown in Fig. 8(a) for LSGM/STO/MgO and (b) for LSGM/$NdGaO_3$ films of different thicknesses, together with data relative to a LSGM polycrystalline pellet that are in agreement with the literature data [6,7]. The difference in transport properties between films and polycrystalline pellet can be attributed to their different microstructures. The large conductivity and low activation energy of LSGM pellet is related to the large grain size (10–20 μm): the bulk contribution prevails on the grain boundary contribution [7,13]. For all samples, conductivity is a function of film thickness, the effect being much more pronounced for the LSGM/STO/MgO films. In detail, conductivity increases with increasing film thickness: for LSGM/STO/MgO films $\sigma = 2.4 \times 10^{-5}$, 3.7×10^{-5}, and 2×10^{-4} Scm^{-1} for 100, 500, and 1000 nm thick films at 600 °C. The corresponding activation energy values show an opposite trend

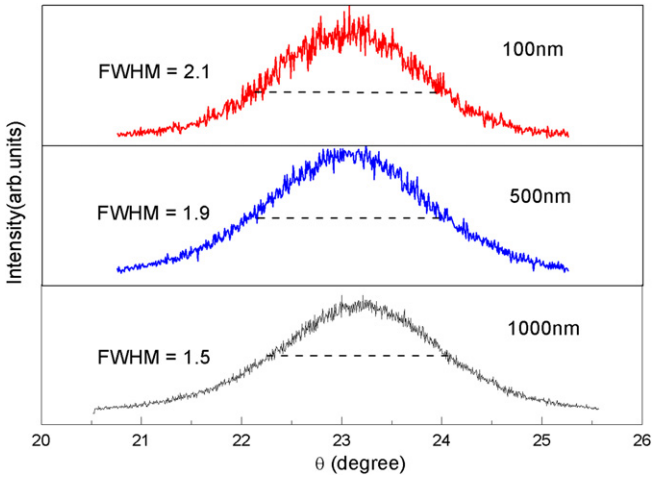

Fig. 6. Rocking-curve scans for as-grown LSGM/STO/MgO films with different thickness.

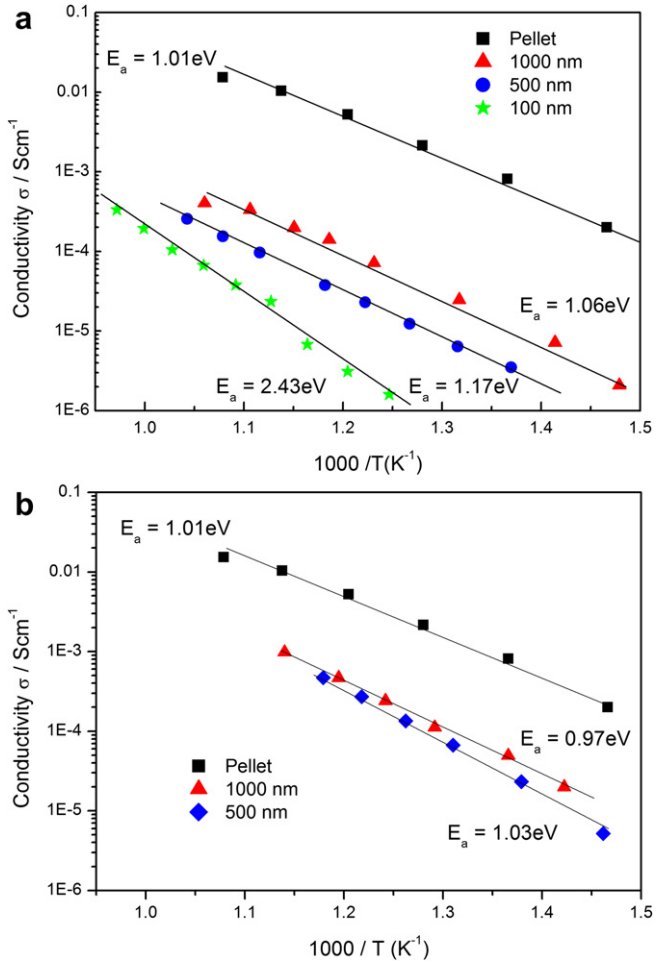

Fig. 8. Arrhenius plots of (a) LSGM/STO/MgO and (b) LSGM/$NdGaO_3$ films of different thicknesses together with LSGM pellet.

E_a = 2.43, 1.17, and 1.06 eV. For LSGM/$NdGaO_3$ films the conductivity values at 600 °C are 1.0×10^{-3} Scm^{-1} and 2.0×10^{-3} Scm^{-1} for 500 and 1000 nm thick films, and the E_a values are 1.03 eV and 0.97 eV, respectively. The E_a of the LSGM 1 μm thick film is very similar to that of the pellet, but its conductivity is much lower.

To understand the observed trends in the films conductivity and activation energy values, both the effect of the substrate/film interface and that of the perpendicular grain boundary should be taken into account and can be analyzed in terms of the space charge layers length [15,16]. The large SCL length, (approximately calculated from conductance *vs* thickness plots to be ca. 80 nm in the present case) is in agreement with previous studies carried out on doped ceria, where the conductivity decrease and associated E_a increase observed with decreasing film thickness has been explained excluding a simple depletion effect at the substrate/film interface and attributed to the concentration of blocking grain boundaries between the columnar structures [11].

In the 'in-plane' geometry used for LSGM thin films, the ionic transport flows parallel to the film surface and thus perpendicular to the main axis of the columnar grains resulting in a lower concentration of grain boundaries defects in thicker films where coalescence of the columnar structures occur [17]. The defects concentration varies roughly from $n \approx 10^{-4}$ nm^{-1} (where n is the inverse of average grain size) in the case of the LSGM pellet, to $n \approx 10^{-2}$ nm^{-1} for the 1 μm thick film. The grain boundary contribution to the total resistivity is thus much larger in thin films than in the sintered pellet. In thicker films, the columnar grains coalescence (grain coarsening) occurring at a later stage of the growth (inset of Fig. 7) results in a higher conductivity.

4. Conclusions

Microstructural studies and XRD data show that LSGM films grown by PLD on $NdGaO_3$ and STO buffered (001) MgO substrate have highly textured, nanocolumnar structure. This effect is mainly observed in LSGM/STO/MgO heterostructures and is a consequence of the large structural misfit between LSGM and MgO only partially accommodated by the STO layer. Columnar grains tend to coalesce as the growth proceeds resulting in a better crystallographic quality for thicker films. Combined analysis of microstructural features and EIS measurements show that the transport properties are dominated by blocking SCLs at the perpendicular grain boundaries of the columnar grains.

Acknowledgments

The authors gratefully acknowledge funding by the Ministry of University and Research (MiUR) of Italy (PRIN Project "PC-SOFCs, Protonic Conductors Solid Oxide Fuel Cells based on nanostructured proton conductors: from materials synthesis to prototype fabrication"). This work was partially supported by META – Materials Enhancement for Technological Applications Project (FP7-PEOPLE-2010-IRSES – Marie Curie Actions, PIRSES-GA-269182).

References

[1] U.P. Muecke, D. Beckel, A. Bernard, A. Bieberle-Hutter, S. Graf, A. Infortuna, P. Muller, J.L.M. Rupp, J. Schneider, L.J. Gauckler, Adv. Funct. Mater. 18 (2008) 3158–3168.
[2] A. Bieberle-Hutter, J.L. Hertz, H.L. Tuller, Acta Mater. 56 (2008) 177–187.
[3] J. Fleig, H.L. Tuller, J. Maier, Solid State Ionics 174 (2004) 261–270.
[4] J.H. Joo, G.M. Choi, J. Eur. Ceram. Soc. 27 (2007) 4273–4277.
[5] A. Tebano, G. Balestrino, N.G. Boggio, C. Aruta, B. Davidson, P.G. Medaglia, Eur. Phys. J. B 51 (2006) 337–340.
[6] T. Ishihara, H. Matsuda, Y. Takita, J. Am. Chem. Soc. 116 (1994) 3801–3803.
[7] M. Feng, J.B. Goodenough, Eur. J. Solid State Inorg. Chem. 31 (1994) 663–667.
[8] F. .Bozza, R. .Polini, E. Traversa, Electrochem. Comm. 11 (2009) 1680–1683.
[9] M. Joseph, P. Manoravi, H. Tabata, T. Kawai, J. Appl. Phys. 92 (2002) 997–1002.
[10] F. Mitsugi, S. Kanazawa, T. Ohkuba, Y. Nomoto, T. Ishihara, Y. Takita, Jpn. J. Appl. Phys. 43 (2004) 299–302.
[11] M.C. Göbel, G. Gregori, X. Guo, J. Maier, Phys. Chem. Chem. Phys. 12 (2010) 14351–14361.
[12] S. Sanna, V. Esposito, D. Pergolesi, A. Orsini, A. Tebano, S. Licoccia, G. Balestrino, E. Traversa, Adv. Funct. Mater. 19 (2009) 1713–1719.
[13] V. Thangdurai, W. Wepper, Electrochim. Acta 50 (2005) 1871–1877.
[14] K. Rodrigo, S. Heiroth, M. Lundberg, N. Bonanos, K. Mohan Kant, N. Pryds, L. Theil Kuhn, V. Esposito, S. Linderoth, J. Schou, T. Lippert, Appl. Phys. A 101 (2010) 601–607.
[15] X. Guo, W. Sigle, J. Fleig, J. Maier, Solid State Ionics 154–155 (2002) 555–561.
[16] D. Gryaznov, J. Fleig, J. Maier, Solid State Sci. 10 (2008) 754–760.
[17] S. Sanna, V. Esposito, A. Tebano, S. Licoccia, E. Traversa, G. Balestrino, Small 5 (2009) 1863–1867.